NANO-OBJECTS IN OWN MATRIX - SELF COMPOSITE

Nebojsa Romcevic*, Maja Romcevic

Institute of Physics Belgrade, University of Belgrade, 11080, Belgrade, Serbia

Abstract

Establishing the principles of nanoscience and nanotechnology has led to rethinking our understanding of the material's properties. Therefore, some earlier results deserve to be analyzed again. In this paper, we present our results, which led to establishing a new type of nanocomposite - Self composite. The Self composite consists of matrix and nanometric size dispersed phase, with the specificity that the nano-object is formed from the same material or its parts, such as a matrix. We have made these nanocomposites using standard methods for the production of monocrystals or molecular beam epitaxy, but slightly above the solubility limit of the starting components. The possibility of obtaining Self composite by laser surface treatment of monocrystalline samples and agglomeration of a part of nanodimensional materials was also presented. Self composites are characterized (SEM, AFM, XRD, far-infrared, and Raman spectroscopy), and results were analyzed by Effective Medium Theory.

Keywords: *nanostructure, nanocomposite, crystal growth, alloy, nano-object*

1. INTRODUCTION

In addition to their excellent features and new properties compared to bulk materials, nanomaterials have many limitations. One of them is that nanoparticles cannot be used on a large scale as long-bearing materials, e.g., for application in the electronic industry. One of the ways to overcome this problem is the development of nanocomposites, which would include nano-objects in the bulk material to obtain new properties. Initial ideas and principles are given in (Dzenis 2008). The advantage of these composites is that the design of new components will be based on the fact that the properties of nanomaterials are unique and significantly different from their bulk relatives from which they are made (Twardowski 2007). Depending on the desired field of application, there are different types of nanocomposites.

If we put nanodimensional ceramic fibers (often a metal) in a ceramic matrix (most often oxides such as nitrides, borides, and silicides), we get Ceramic matrix composites (CMCs). For these composites to have good optical, electrical and magnetic properties (Kruis, Fissan & Peled 1998) and be acceptable for use in industry (e.g., corrosion protection (Zhang et al. 2005)), the technological process of their production must ensure a homogeneous distribution of ceramic fibers within the matrix.

To take advantage of the exceptional properties of carbon nanotube materials (Dawid & Barbara 2018), such as high tensile strength and electrical conductivity, Carbon nanotube metal matrix composites CNT-MMC, which are part of a large group of Metal matrix nanocomposites, are intensively developed. Ensuring a homogeneous dispersion of nanotubes in the metal matrix, a strong connection between the metal matrix and carbon nanotubes, and economic justification are the requirements that this class of nanocomposites must fulfil to play a more significant role in the industry. Until then, this is just a new area of scientific research (Dawid & Barbara 2018).

A good feature of nanocomposite is that it is enough that one part of it, e.g., dispersed phase, is sensitive to external influences, e.g., magnetic or electric field. Magnetic nanocomposites are a good example. Various nano-objects can be added relatively without difficulty to the non-magnetic matrix (Silke & Ingo 2016).

Polymer nanocomposites are very popular. In them, semiconductor nano-objects (inorganic component) are dispersed in an organic polymer matrix. This type of nanocomposite shows how the limitations of one material can be improved by another constituent element (Tamborra et al. 2004). For

example, polymers that have deficiencies in mechanical, thermal, and electronic properties show satisfactory characteristics for application as nanocomposites with appropriate functionalization.

Our research is based on the fact that the same material in the bulk form and as a nanodimensional material has significantly different characteristics. Therefore, viewed from the side of the composite material, the bulk material and its nanodimensional relative represent two different materials. Based on that, in this paper, we present our earlier results as a review, which led to establishing a new type of nanocomposite that consists of a matrix (which can be of any material) and nanometric size dispersed phase, with the specificity that the nano-object is formed from the same material, or its parts, such as a matrix - Self composite.

2. MATERIALS AND METHODS

We focused on semiconductor single crystal solid solutions of the $AB_{1-x}C_x$ type or similar compounds, which were synthesized from the starting components - elementary substances, binary compounds AB, AC, etc. Sometimes, these solid solutions do not exist for every value of x, i.e., the solubility of one phase into the other is limited. Under certain conditions, the excess of component AC in the starting mixture slightly above the limit of its solubility will cause the formation of the solid solution with the dispersed AC phase in the form of the nano-objects, i.e. self composite was formed.

We have made our Self composites (matrix/dispersed phase) by two approaches:

1. Using standard methods for the production of monocrystals–Czochralski, Bridgman, and direct fusion method (example $Hg_{1-x}Mn_xTe_{1-y}Se_y$/MnSe, $Zn_{1-x}Mn_xSnAs_2$/MnAs and $Cd_{1-x}Mn_xSnAs_2$/MnAs), or molecular beam epitaxy ($Pb_{1-x}Mn_xTe$/MnTe and $Cd_{1-x}Mn_xTe$/MnTe) for the production of the thin films, but slightly above the solubility limit of the starting components;

2. Laser material treatment; here we have two possibilities:

a) If we treat a monocrystalline sample with a laser, nano-objects will be formed on the surface;

b) In the case of laser treatment of nanoparticles, agglomeration of nanoparticles into amorphous or crystalline structure will occur, and under carefully selected conditions, a certain amount of isolated nanoparticles will remain.

Synthesized Self composites are characterized by standard methods such as SEM, AFM, XRD, FIR and Raman spectroscopy.

2.1. Results and Discussion, Examples of Self Composites

2.1.1. HgMnTeSe/MnSe

HgMnTeSe samples were grown by the modified Bridgman technique from chemically pure components. We investigate a lot of samples (Romcevic & Romcevic 2003; Romcevic et al. 2005; Romcevic et al. 2009; Petrovic et al. 2012; Jovanovic et al. 2005; Romcevic et al. 2005). We singled out the composition $Hg_{0.91}Mn_{0.09}Te_{0.9}Se_{0.1}$/MnSe, where the total concentration of Se does not exceed 11%. Of this, about 10% enters the solid solution, and 1% remains undissolved.

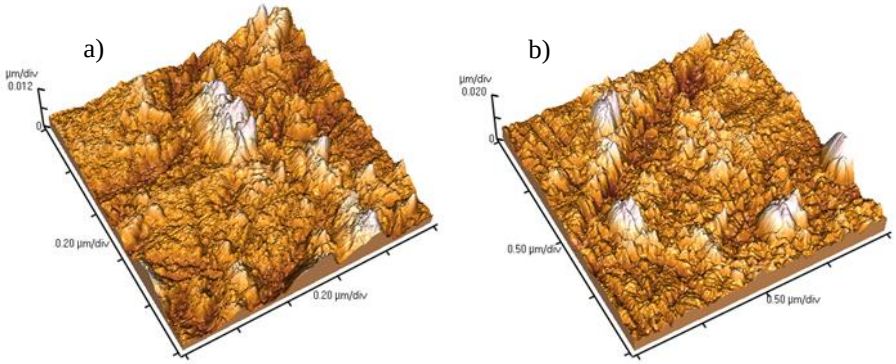

Fig. 1. AFM images of the surface of the: (a) $Hg_{0.95}Mn_{0.05}Te_{0.9}Se_{0.1}$; (b) $Hg_{0.91}Mn_{0.09}Te_{0.9}Se_{0.1}$/MnSe mixture.

The corresponding AFM images are shown in Fig.1 to see the difference in the morphology of the single crystal HgMnTeSe sample and the sample in which the Self composite $Hg_{0.91}Mn_{0.09}Te_{0.9}Se_{0.1}$/MnSe was formed. The image of a single crystal sample is standard for this type of material (Petrovic et al. 2012). In Self composite obtained by crystal growth, slightly above Mn and Se solubility limit, we see an additional structure (300 nm in diameter and 40 nm in height). This means that the excess Mn and Se did not dissolve and form a monocrystalline structure but separated and formed a nano-object.

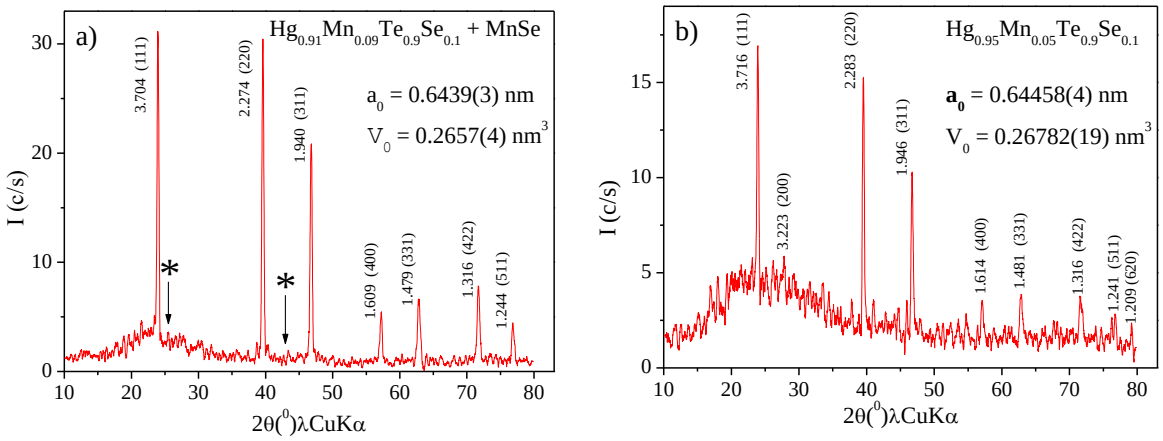

Fig. 2. XRD spectra of the: a) $Hg_{0.91}Mn_{0.09}Te_{0.9}Se_{0.1}$ + MnSe mixture, b) $Hg_{0.95}Mn_{0.05}Te_{0.9}Se_{0.1}$.

The diffractograms from Figs.2a and 2b confirm this. The peaks marked with an asterisk, which exist only in the Self composite (Fig.2a) and are absent in the single crystal sample (Fig.2b), correspond to cubic MnSe (JCPDS card 27-0311).

Fig. 3a shows the characteristic far-infrared spectra of single crystal $Hg_{1-x}Mn_xTe$ and $Hg_{1-x}Mn_xTe_{1-y}Se_y$ samples which are analyzed in detail in our papers (Romcevic & Romcevic 2003; Romcevic et al. 2005; Romcevic et al. 2009; Petrovic et al. 2012; Jovanovic et al. 2005; Romcevic et al. 2005). The theoretical models used are standard (Romcevic et al. 2005). In short, the shape of the spectrum depends on the value of the energy gap, first of all. In addition, characteristics derived from binary components (HgTe or MnTe), and impurity (Mn, Se), as characteristic frequencies of single crystals, are seen.

The far-infrared spectrum of the $Hg_{0.91}Mn_{0.09}Te_{0.9}Se_{0.1}$/MnSe Self Composite (Fig. 3b) is significantly different from the spectra of single crystal samples from Fig. 3a. Therefore, the model used for Fig. 3a does not give good results (see the range from 250 to 350 cm^{-1}). However, it is entirely appropriate to use the Effective Medium Theory (Sihvola 1999). In our case, nano-objects are spheres with volume fraction f ($f=4\pi na^3/3$, a is the diameter of the sphere), which consist of α-MnSe and β-MnSe (dielectric functions ε_i), which are dissolved in single crystal HgMnTeSe (dielectric functions ε_b). This gives the effective dielectric function:

$$\varepsilon_{eff} = \varepsilon_b + \frac{3f\varepsilon_b(\varepsilon_i - \varepsilon_b)}{\varepsilon_i + 2\varepsilon_b - f(\varepsilon_i - \varepsilon_b)} \quad (1)$$

This approach led to an excellent match between the experimental and theoretical spectra, as seen in Fig. 3c. The proportion of nano-objects in the Self composite of 5% was also precisely determined. We think that in this way, the existence of MnSe nano-objects in the HgMnTeSe matrix has been proved.

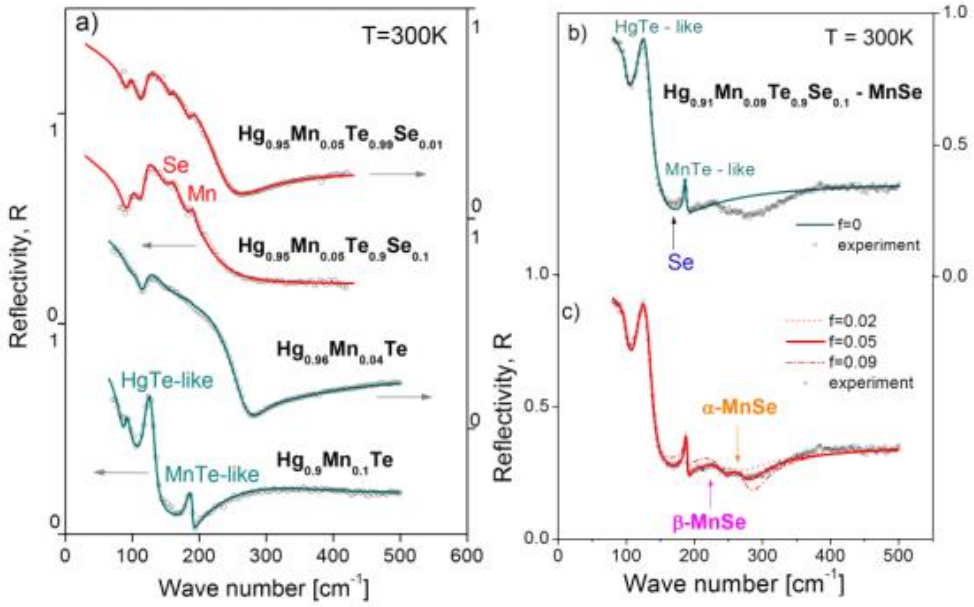

Fig. 3. Far-infrared reflection spectra of a) different $Hg_{1-x}Mn_xTe_{1-y}Se_y$. The solid line is a calculated spectrum obtained by a fitting procedure (Petrovic et al. 2012); b) $Hg_{0.91}Mn_{0.09}Te_{0.9}Se_{0.1}$/MnSe mixture. c) $Hg_{0.91}Mn_{0.09}Te_{0.9}Se_{0.1}$/MnSe mixture. The lines are calculated spectra obtained by a fitting procedure based on the model given by Eq.(1) for different f.

2.1.2. $Pb_{1-x}Mn_xTe$/MnTe

$Pb_{1-x}Mn_xTe$ was analyzed similarly. We analyzed the phonon properties, plasmon-phonon interaction, and surface effects of many single crystals, thin films, and structures (Romcevic et al. 1997; Romcevic et al 1997; Romcevic, Romcevic & Nikiforov 2001; Trajic et al. 2004; Romcevic et al. 2005; Romcevic et al. 2007; Trajic et al. 2007; Radisavljevic et al. 2013). Here we will pay attention to the results for thin films obtained by the MBE process slightly above the solubility limit Mn, i.e., $x > 0.12$. $Pb_{1-x}Mn_xTe$ layers (0.75 - 4.5 μm) were deposited on BaF_2 or KCl substrates and PbTe buffer layer (0.1–0.4 μm).

3D AFM images are very useful in analyzing the surface of thin films, as seen in Fig. 4a-c. Thus, for thin films of Self Composite PbMnTe on BaF_2 and KCl substrate, which is our case, the characteristics of undissolved MnTe are clearly visible. The dimensions of these islands depend on the type of

substrate. In the case of KCl, they are twice as large as for BaF_2, where they are about 40 nm wide. Larger structures (150 nm wide) belong to the PbMnTe thin film, which is usual in this case (Romcevic et al. 2007).

The far-infrared spectrum of $Pb_{0.88}Mn_{0.12}Te$ single crystal (Fig. 4d) shows all the characteristics of the phonon spectrum that three-component alloys have (Romcevic & Romcevic 2006), as well as the effects associated with plasmon-phonon interaction (Trajic et al. 2004). The same applies to the far-infrared spectra of BaF_2 and the spectrum of a thin film of PbTe on a BaF_2 substrate (Romcevic et al. 2007), which were analyzed in a standard way for this group of materials (Gilic et al. 2013). The far-infrared reflectivity spectrum of the BaF_2 substrate is shown at the bottom of Fig. 4e. As a result of the best fit, we obtained the ω_{TO} = 190 cm^{-1} and ω_{LO} = 338 cm^{-1}, the same as the literature data (Romcevic et al. 2007). The far-infrared spectra of PbTe thin film on BaF_2 substrate are shown at the middle of Fig. 4e. The schematic picture of that sample, with characteristic parameters, is presented, also. The vertical dashed line denotes the position of ω_{TOBaF2} mode. Despite the strong plasmon-LO phonon coupling, we obtain the well-known parameters for PbTe: ω_{TO} =32 cm^{-1} and ω_{LO} = 104 cm^{-1}. The position of registered interference minima is directly connected with the thickness of PbTe film.

For the Self Composite spectra (Fig. 4e top), the Effective Medium Theory for the final PbMnTe layer must be used. The displayed spectrum carries with it the properties of both the substrate and the buffer layer. In comparison with the spectrum of PbMnTe single crystals, we clearly see a new structure.The TO/LO characteristics of the additional structure at 135/190cm^{-1} are obtained, and corresponding to MnTe (NiAs structure) as given in (Romcevic et al. 2007).

It seems to us that in this way, the existence of the $Pb_{0.88}Mn_{0.12}Te$ layer with MnTe nano-objects in it has been proved, i.e., we have Self composite here too.

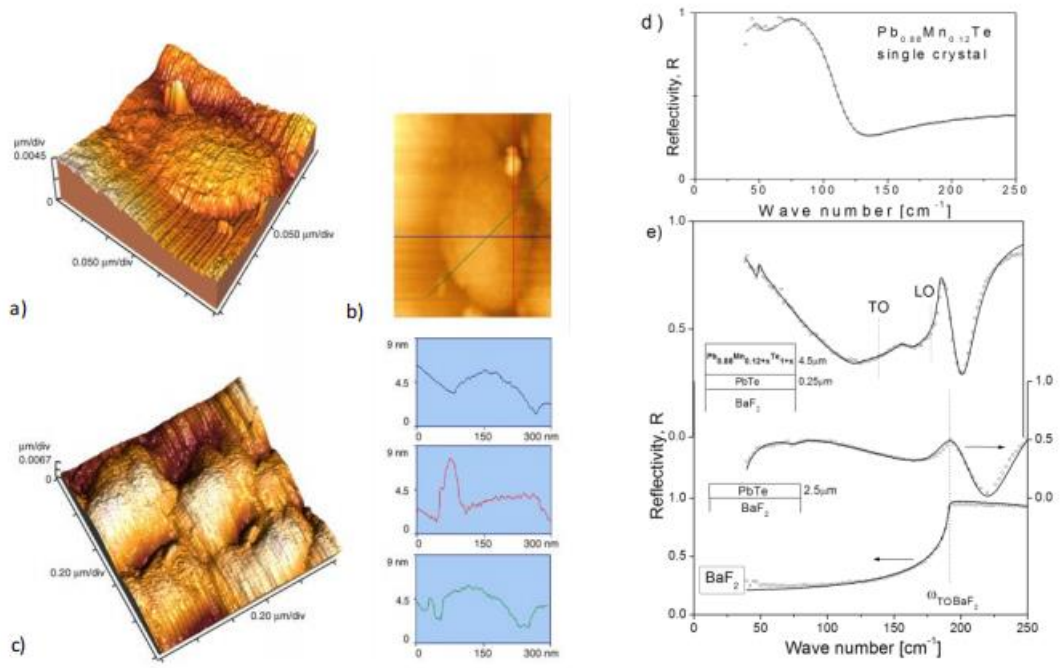

Fig. 4. a) 3D AFM image of PbMnTe layers on BaF_2 substrate; b) 2D AFM image of PbMnTe layers on BaF_2 substrate; c) 3D AFM image of PbMnTe layers on KCl substrate. d) Far-infrared reflection spectra of $Pb_{0.88}Mn_{0.12}Te$ single crystal. e) Far-infrared reflection spectra of BaF_2, PbTe on BaF_2 substrate and $Pb_{0.88}Mn_{0.12+x}Te_{1+x}$ ($Pb_{0.88}Mn_{0.12}Te$/MnTe) thin films on PbTe buffer layers and BaF_2 substrate.

2.2. Laser modification of single crystals and nanoparticles

Lasers and laser technology are very prominent in modifying single crystal surfaces (Ed. by Schaaf 2010). The degree of modification and the thickness of the layer on the surface in which this modification occurs depend on the type of material and the wavelength, power, duty cycle, and repetition rate of the laser beam (Shugaev 2016).

In our previous papers, we have investigated the influence of locally induced heating with increasing laser power densities on some nanomaterials, such as stable hexagonal transition oxide ZnO doped with CoO (Hadzic 2016) and cubic rock-salt MnO (Hadzic 2018; Babic 2019). In addition, the influence of laser power on the quality and optical characteristics of $Bi_{12}GeO_{20}$ single crystal was also studied. (Kovacevic 2016)

From the point of view of Self composite formation, the most illustrative example is the laser treatment of MnO nanoparticles. Polycrystalline MnO sample powder was purchased from Sigma-Aldrich Co. Verdi G optically pumped semiconductor laser operating on 532 nm laser line with 15 mW power was used.

The topography of the MnO sample was investigated by AFM measurements and shown in Fig. 5a insert. In these images, it is notable that the untreated sample has a grain structure, with grain size below 1 μm. After laser irradiation, changes are examined in sample topography. One can see, in these pictures that grain structure disappears. Aggregates of adjacent grains are then transformed into either a larger bump or a relatively flat surface. Very few microstructures remain undissolved.

XRD spectroscopy (see Fig. 5b insert) confirms the AFM results. Different MnO phases were registered (MnO, MnO_2 and Mn_3O_4), as well as the α phase of elemental Mn, with the crystalline size varying between 18.7 and 25.6 nm. Obtained XRD results confirm that laser irradiation produced a permanent change in the sample. From the existence of α- phase elemental Mn after laser irradiation, we can conclude that laser-induced local heating on the sample surface hasn't raised the temperature on the sample surface over 1000 K.

As in the previous cases, the far-infrared and Raman spectra differ significantly for the sample that has Self composite and the one that is the base material. Here, that difference is registered for the sample treated with a laser and the one that did not have laser treatment, shown in Fig. 5a (far-infrared spectra) and Fig. 5b (Raman spectra). In addition to the properties of MnO nanoparticles, the MnO phases that were created due to the laser action are now registered and represent the matrix in which there are nano-objects.

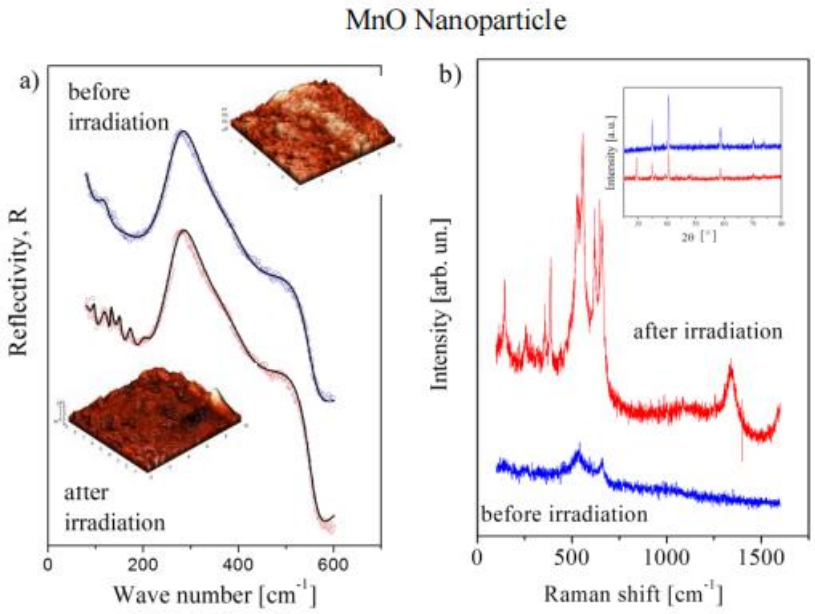

Fig. 5. a) Far-infrared spectra of the MnO sample. Isert: Atomic force microscopy topography before and after irradiation. b) Raman spectra of MnO sample before and after laser irradiation. Insert: X–ray diffraction spectra of MnO sample before and after laser irradiation.

This way of obtaining Self composite is very sensitive to the applied laser power and the length of the treatment, and all of this is related to the type of nanoparticles to which the treatment is applied.

These materials' functionality and potential application in optics, magneto-optics, and the field of thermoelectric materials were examined. It will be possible to find a place for the new nanocomposites of our type (Self composite) in all industrial areas where monocrystals and polycrystals are obtained using Czochralski, Bridgeman, and other similar methods are used. In a practical sense, that will be the application of the well-known but qualitatively new material with a new, more comprehensive range of functionality. They can be managed during the production of nanocomposites or later while incorporating these materials as, for example, sensors or active elements.

3. CONCLUSIONS

Using nanomaterials in robust electronics and related industries requires a new approach. This paper is dedicated to our earlier results that led us to investigate new nanocomposites that consist of a matrix (any material) and nanometric size dispersed phase, with the specificity that the nano-object is formed from the same material or its parts, such as a matrix. Semiconducting nanomaterials are very suitable for this type of composite. They are obtained by classical methods and can find application in all areas where they are used in the form of single crystals. We think this nanocomposite class is very perspective for applications, and these nanocomposites have unique characteristics, so they should be singled out as a special one - Self composite.

ACKNOWLEDGMENTS

This research was supported by the Science Fund of the Republic of Serbia, Grant No. 7504386, Nano object in own matrix – Self composite – NOOM-SeC.

REFERENCES

1. Dzenis, Y 2008, „Structural Nanocomposites“, *Science* vol. 319, pp. 419-420.
2. Twardowski, TE 2007, “Introduction to Nanocomposites Material Properties, Processing, Characterization”, *Destech Publications*, Lancaster, Pa, USA, pp. 1.
3. Kruis, FE Fissan, H & Peled, A 1998, „Synthesis of nanoparticles in the gas phase for electronic, optical and magnetic applications“, *J. Aerosol Sci.* Vol. 29, no. (5–6), pp. 511-535.
4. Zhang, S Sun, D Fu, Y & Du, H 2005, „Toughening of hard nanostructural thin films: a critical review“, *Surf. Coat. Technol.* vol. 198, no. (1–3), pp. 2-8.
5. Dawid, J & Barbara, L 2018, „Copper matrix nanocomposites based on carbon nanotubes or graphene“, *Mater. Chem. Front.* vol. 2, pp. 22-35.
6. Silke, B & Ingo, A 2016, „Systems biology - Nanobiotechnology“, *Current Opinion in Biotechnology* vol. 39, pp. 1-122.
7. Tamborra, M Striccoli, M Comparelli, R Curri, ML Petrella, A Agostiano, A 2004,“ Optical properties of hybrid composites based on highly luminescent CdS nanocrystals in polymer“, *Nanotechnology* vol. 15, no. 4, pp. S240.
8. Romcevic, M & Romcevic, N 2003, „Far-infrared spectra of $Hg_{1-x}Mn_xTe$ alloys“, *Infrared Phys. & Technology* vol. 44, pp. 35-41.
9. Romcevic, M Kulbachinskii, VA Romcevic, N Maryanchuk, PD & Churilov, IA 2005, „Optical Properties of $Hg_{1-x}Mn_xTe_{1-y}Se_y$, *Infrared Phys. & Technology* vol. 46, pp. 379-387.
10. Romcevic, N Romcevic, M Milutinovic, A & Kostic, S 2009, „Plasmon-phonon interaction in $Hg_{1-x}Mn_xSe$ alloys“, *Journal of Alloys and Compounds* vol. 478, pp. 41-44.
11. Petrovic, M Romcevic, N Romcevic, M Stanisic, G Vasiljevic-Radovic, D Trajic, J Lazarevic, Z & Kostic, S 2012, „Spectroscopy characterization of MnSe nanoclasters randomly distributed in HgMnTe single crystal“, *Journal of Crystal Growth* vol. 338, pp. 75-79.
12. Jovanovic, D Milivojevic, D Romcevic, M Babic-Stojic, B & Romcevic, N 2005, „Optical and Magnetic Properties of $Hg_{1-x}Mn_xSe$ Alloys“, *Materials Science Forum* vol. 494, pp. 277-282.
13. Romcevic, N Romcevic, M Golubovic, A Khoi, LV Mycielski, A Jovanovic, D Stojanovic, D Nikolic, S & Duric, S 2005, „Far-infrared and Raman spectroscopy of $Cd_{1-x}Mn_xTe_{1-y}Se_y$: Phonon properties“, *Journal of Alloys and Compounds* vol. 397, pp. 52-57.
14. Sihvola, A 1999, „Electromagnetic Mixing Formulae and Applications“, (IEEE Electro-magnetic Waves Series 47) pp. 1–274.
15. Romcevic, N Popovic, ZV Khokhlov, D Ivanchik, II Nikorich, AV & König, W 1997, „Vibrational spectroscopy of indium-doped $Pb_{0.9}Mn_{0.1}Te$ alloy“, *Zeitschrift für Physik B* vol. 104, pp. 475-480.
16. Romcevic, N Popovic, ZV Khokhlov, D & König, W 1997, „Far-infrared spectroscopy of localized states in indium doped PbTe and $Pb_{1-x}A_xTe$ (A_x=$Mn_{0.017}$; $Sn_{0.18}$) alloys“, *Infrared Phys. & Technology* vol. 38, pp. 117-122.
17. Romcevic, M Romcevic, N & Nikiforov, VN 2001, „Far-infrared spectra of $Pb_{1-x}Mn_xTe$ alloys“, *Infrared Phys. & Technology* vol. 42, pp. 541-545.
18. Trajic, J Romcevic, M Romcevic, N Nikolic, S Golubovic, A Duric, S & Nikiforov, VN 2004, „Optical properties of PbTe:Mn“, *Journal of Alloys and Compounds* vol. 365, pp. 89-93.
19. Romcevic, N Golubovic, A Romcevic, M Trajic, J Nikolic, S Duric, S & Nikiforov, VN 2005, „Raman spectra of $Pb_{1-x}Mn_xTe$ alloys“, *Journal of Alloys and Compounds* vol. 402, pp. 36-41.

20. Romcevic, N Nadolny, AJ Romcevic, M Story, T Taliashvili, B Milutinovic, A Trajic, J. Lusakowska, E Vasiljevic-Radovic, D Domukhowski, V Osinniy, V Hadzic, B & Dziawa, P 2007, „Far-infrared phonon spectroscopy of $Pb_{1-x}Mn_xTe$ layers grown by molecular beam epitaxy“, *Journal of Alloys and Compounds* vol. 438, pp. 34-40.
21. Trajic, J Romcevic, N Romcevic, M & Nikiforov, VN 2007, „Plasmon - phonon and plasmon - two different phonon interaction in $Pb_{1-x}Mn_xTe$ mixed crystals“, *Materials Research Bulletin* vol. 42, pp. 2192-2201.
22. Radisavljevic, I Novakovic, N Mahnke, H'E Romcevic, N Medic, M Paskas-Mamula, B & Ivanovic, N 2013, „X-ray absorption near edge structure studies of $Pb_{1-x}Mn_xTe$(In, Ga) systems“, *International Journal of Materials Research* vol. 104, no. 3, pp. 319-325.
23. Romcevic, M & Romcevic, N 2006, „Phonons in multicomponent alloys“, *Journal of Alloys and Compounds* vol. 416, pp. 64-71.
24. Gilic, M Trajic, J Romcevic, N Romcevic, M Timotijevic, DV Stanisic, G & Yahia, IS 2013, „Optical properties of CdS thin films“, *Optical Materials* vol. 35, pp. 1112-1117.
25. Ed. by Schaaf, P 2010, "Laser Processing of Materials", (Springer Series in Materials Science (SSMATERIALS,) Vol. 139.
26. Shugaev, MV Wu, C Armbruster, O Naghilou, A Brouwer, N Ivanov, DS Derrien, TJ-Y Bulgakova, NM Kautek, W Rethfeld, B & Zhigilei, LV 2016, „Fundamentals of ultrafast laser–material interaction“, *MRS Bulletin* vol. 41, no. 12, pp. 960-968.
27. Hadzic, B Romcevic, N Sibera, D Narkiewicz, U Kurylisyn-Kudelska, I Dobrowolski, WD & Romcevic, M 2016, „Laser power influence on Raman spectra of ZnO(Co) nanoparticles“, *Journal of Physics and Chemistry of Solids* vol. 91, pp. 80-85.
28. Hadzic, B Vasic, B Matovic, B Kuryliszyn-Kudelska, I Dobrowolski, WD Romcevic, M & Romcevic, N 2018, „Influence of laser induced heating on MnO nanoparticles“ *Journal of Raman Spectroscopy* vol. 49, no. 5, pp. 817-821.
29. Babic, B Hadzic, B Kuryliszyn-Kudelska, I Paunovic, N Vasic, B Dobrowolski, WD Romcevic, M Trajic, J & Romcevic, N 2019, „Far-infrared spectroscopy of laser power modified MnO nanoparticles“, *Optoelectronics and Advanced Materials - Rapid Communications* vol. 13, no. 5-6, pp. 376-379.
30. Kovacevic, A Ristic-Djurovic, J Lekic, M Hadzic, B Abudagel, GSI Petricevic, S Mihailovic, P Matovic, B Dramlic, D Brajovic, Lj & Romcevic, N 2016," Influence of femtosecond pulsed laser irradiation on bismuth germanium oxide single crystal properties“, *Materials Research Bulletin* vol. 83, pp. 284-289.